Flavor structure of the nucleon electromagnetic form factors and transverse charge densities in the chiral quark–soliton model

António Silva[1,2,*], Diana Urbano[1,*], and Hyun-Chul Kim[3,4,*]

[1]*Departamento de Engenharia Física, Faculdade de Engenharia, Universidade do Porto, rua Dr. Roberto Frias, 4200-465 Porto, Portugal*
[2]*Centro de Física do Porto, Faculdade de Ciências da Universidade do Porto, Rua do Campo Alegre 687, 4169-007 Porto, Portugal*
[3]*Department of Physics, Inha University, Incheon 402-751, Korea*
[4]*School of Physics, Korea Institute for Advanced Study (KIAS), Seoul 130-722, Republic of Korea*
*E-mail: ajsilva@fe.up.pt; urbano@fe.up.pt; hchkim@inha.ac.kr

....
We investigate the flavor decomposition of the electromagnetic form factors of the nucleon, based on the chiral quark–soliton model (χQSM) with symmetry-conserving quantization. We consider the rotational $1/N_c$ and linear strange-quark mass (m_s) corrections. We discuss the results of the flavor-decomposed electromagnetic form factors in comparison with the recent experimental data. In order to see the effects of the strange quark, we compare the SU(3) results with those of SU(2). Finally, we discuss the transverse charge densities for both unpolarized and polarized nucleons. The transverse charge density inside a neutron turns out to be negative in the vicinity of the center within the SU(3) χQSM, which can be explained by the contribution of the strange quark.
....

Subject Index   D32

1. Introduction

Electromagnetic form factors (EMFFs) are the most fundamental observables that reveal the charge and magnetization structures of the nucleon. A series of recent measurements of the EMFFs has renewed the understanding of the internal structure of the nucleon and has posed fundamental questions about its nonperturbative nature. The results of the ratio of the proton EMFFs, $\mu_p G_E^p / G_M^p$ with the proton magnetic moment μ_p, obtained by measuring the transverse and longitudinal recoil proton polarizations [1–8], were found to decrease almost linearly with Q^2 above 1 $(\mathrm{GeV}/c)^2$. These results were in conflict with most of the previous measurements of the proton EMFFs from unpolarized electron–proton cross sections based on the Rosenbluth separation method. These new experimental results have triggered subsequent theoretical and experimental works (see, e.g., Refs. [9–13]). This discrepancy is partially explained by the effects of two-photon exchange, which affects unpolarized electron–proton scattering at higher Q^2 but has less influence on the polarization measurements [14–19]. Moreover, the new experimental results of the proton EMFFs in a wider range of Q^2 provided a whole new perspective on the internal quark–gluon structure of the nucleon. Perturbative quantum chromodynamics (pQCD) with factorization schemes [20] predicts the different scalings of the Dirac and Pauli FFs, F_1^p and F_2^p: F_1^p falls off as $1/Q^4$ while F_2^p decreases as $1/Q^6$, so that

$Q^2 F_2^p / F_1^p$ becomes flat at large Q^2. However, the experimental data show that the ratio $Q^2 F_2^p / F_1^p$ increases with Q^2 but $Q F_2^p / F_1^p$ becomes flat starting around $2\,\mathrm{GeV}^2$. A similar discrepancy between the experimental data and pQCD was also found in the $\gamma \gamma^* \to \pi$ transition form factor [21,22], even for higher Q^2. This implies that it is far more important to consider effects from nonperturbative physics than those from perturbative QCD in the lower Q^2 region.

Assuming isospin and charge symmetries, neglecting the strangeness in the nucleon, and using both the experimental data for the proton and neutron EMFFs, Cates et al. [23] have extracted the up and down EMFFs and have obtained remarkable results: the Q^2 dependences of the up- and down-quark Dirac (F_1) and Pauli (F_2) form factors (FFs) are considerably different from each other. The down-quark Dirac and Pauli FFs are roughly proportional to $1/Q^4$ but those of the up quark fall off more gradually. Moreover, while the ratios $\kappa_u^{-1} F_2^u / F_1^u$ and $\kappa_d^{-1} F_2^d / F_1^d$ (κ is the anomalous magnetic moment) are relatively constant above $Q^2 \sim 1\,\mathrm{GeV}^2$, they show a complicated behavior for lower Q^2 regions. Qattan and Arrington [24,25] elaborated on the analysis of Ref. [23], taking into account explicitly the effects of two-photon exchange and uncertainties on the proton form factor and the neutron magnetic FFs. They found that the ratio of the up-quark EMFFs (G_E^u / G_M^u) has a roughly linear drop-off, while that of the down-quark EMFFs (G_E^d / G_M^d) showed a completely different dependence on Q^2. As a result, the flavor-decomposed FFs behave in a different way to the proton EMFFs. Diehl and Kroll [26] critically analyzed experimental data in order to study several hadron properties and also obtained a separation of the light quark contributions to form factors. The flavor contributions to the EMFFs of the nucleon and the related charge and magnetization densities had already been a subject of interest prior to the phenomenological analysis of Refs. [23] and [24,26]: Ref. [27] used a framework based on the Faddeev equation with dressed quarks to obtain the flavor contributions to the Dirac, Pauli, and Sachs form factors, including the associated radii, while Ref. [28] used a vector dominance model. These studies, as well as experimental results [29], pointed out the nontrivial behavior of these contributions, as revealed further by the analysis of Refs. [23,24,26]. Several theoretical studies of these contributions have since been performed: Ref. [30] further developed the covariant Faddeev framework, based on the Dyson–Schwinger equations of QCD; Refs. [31,32] employed a Goldstone-boson-exchange relativistic constituent quark model; and Ref. [33] extended the quark–diquark model to include a pion cloud. The flavor contributions to the EMFFs were obtained in Ref. [34] by computing the generalized parton distributions in a reggeized diquark model and in Ref. [35] from generalized parton distributions obtained in a quark model in AdS/QCD. The AdS/QCD correspondence has been the basis for similar studies within different approaches: in a light-front quark model in a soft-wall model [36] or a hard-wall model [37], and also via parametrization approaches [38,39]. Reference [40] used the light-front holographic QCD framework including higher Fock components; Ref. [41] a relativistic light-front model. The flavor contributions may equally be displayed through the transverse charge and magnetization densities, as one may find in Refs. [42,43], which employed a soft-wall model of AdS/QCD, and also in some of the aforementioned studies.

In this context, we investigated the flavor structure of the nucleon EMFFs within the framework of the self-consistent SU(2) and SU(3) chiral quark–soliton models (χQSMs) [44–46]. The χQSM has successfully described various observables of the baryon octet and decuplet (for reviews, see Refs. [47–50]). In particular, the Q^2 dependence of almost all form factors is well reproduced within the χQSM, so that the strange-quark EMFFs [51] and the parity-violating (PV) asymmetries of polarized electron–proton scattering [52], which require nine different FFs (six EMFFs and three axial-vector FFs) with the same set of parameters, are in good agreement with experimental data.

Thus, it is worthwhile to examine the flavor structure of the nucleon EMFFs in detail. As mentioned, the nucleon EMFFs have already been studied in the SU(3) χQSM [53]. However, Praszałowicz et al. [54] pointed out that the Gell-Mann–Nishijima relation was not exactly fulfilled in the initial version of the χQSM and proposed the symmetry-conserving quantization that makes the Gell-Mann–Nishijima relation well satisfied. We want to emphasize that the χQSM is a reasonable framework to investigate the properties of the lowest-lying SU(3) baryons. Witten originally proposed in his seminal papers [55–57] that the lowest-lying light baryons may be regarded as bound states of N_c *valence* quarks in a meson mean field. In the limit of the large number of colors (N_c), the lowest-lying SU(3) baryons constitute N_c *valence* quarks that bring about an effective pion mean field or the vacuum polarization. The value of N_c will be taken to be three at the final stage of the computation such that we are able to compare the present results with the experimental data. Recently, this mean-field approach or the χQSM have successfully described properties of singly heavy baryons [58–60].

In this work, we present the results of the flavor-decomposed up- and down-quark EMFFs based on the SU(3) χQSM with symmetry-conserving quantization employed. We first show the Dirac and Pauli FFs of the nucleon and then examine the Q^2 dependence of the up- and down-quark Dirac and Pauli FFs. The ratio of the flavor-decomposed Dirac and Pauli FFs will be discussed, compared with the recent experimental data [24]. We also reexamine the results of the strange EMFFs, since there are new experimental data from PV polarized electron–nucleon scattering. In particular, the G0 Collaboration recently measured the parity-violating asymmetries in the backward angle [61], which was first predicted in Ref. [52]. In addition to the flavor-decomposed EMFFs of the nucleon, we also investigate the charge and magnetization densities of the quark in a nucleon in the transverse plane. Together with the new experimental data for the nucleon EMFFs, the nucleon GPDs (generalized parton distributions) cast light on the concept of nucleon FFs [50,62–64].

The present work is sketched as follows. In Sect. 2, we briefly review the general formalism of the EMFFs of the nucleon and its flavor decomposition and describe how to compute the EMFFs of the nucleon within the framework of the SU(2) and SU(3) χQSMs. In the following sections we present the results and discuss their physical implications in the light of the recent experimental data: for Sachs FFs in Sect. 3 and for the Dirac and Pauli FFs in Sect. 4. In Sect. 5 we also present the model results for the transverse charge and magnetic distributions of the quark inside both unpolarized and transversely polarized nucleons. The final section is devoted to the summary and the conclusions.

2.   Electromagnetic form factors and the χQSM

The matrix element of a flavor vector current between the two nucleon states is expressed in terms of the flavor Dirac and Pauli FFs:

$$\langle N(p', s')|J_\mu^\chi(0)|N(p, s)\rangle$$
$$= \bar{u}_N(p', s')\left[\gamma_\mu F_1^\chi(q^2) + i\sigma_{\mu\nu}\frac{q^\nu}{2M_N}F_2^\chi(q^2)\right]u_N(p, s), \tag{1}$$

where $J_\mu^\chi(0)$ represents the flavor vector current defined as

$$J_\mu^\chi(0) = \bar{\psi}(0)\lambda^\chi\gamma_\mu\psi(0). \tag{2}$$

χ denotes the flavor index, i.e., $\chi = 0, 3, 8$ for the flavor decomposition. Here, one has to bear in mind that λ^0 is considered to be a unity flavor matrix. Thus, the normalization $\{\lambda^a, \lambda^b\} = 2\delta^{ab}$ for

λ^χ applies only to the Gell-Mann matrices with $\chi = 3$ and $\chi = 8$. The Dirac spinor $u_N(p, s)$ applies to the nucleon with mass M_N, momentum p, and the third component of its spin s. The square of the four momentum transfer is denoted by $q^2 = -Q^2$, with $Q^2 > 0$. The flavor Dirac and Pauli FFs can be combined to give the Sachs FFs:

$$G_E^\chi(Q^2) = F_1^\chi(Q^2) - \frac{Q^2}{4M_N^2}F_2^\chi(Q^2)$$

$$G_M^\chi(Q^2) = F_1^N(Q^2) + F_2^\chi(Q^2). \tag{3}$$

In the Breit frame, $G_E^\chi(Q^2)$ and $G_M^\chi(Q^2)$ are related to the time and space components of the flavor vector current, respectively:

$$G_E^\chi(Q^2) = \langle N'(p')|\bar{\psi}(0)\gamma_0\lambda^\chi\psi(0)|N(p)\rangle$$

$$G_M^\chi(Q^2) = iM_N\epsilon_{ilk}\frac{q_l}{6q^2}\mathrm{tr}\left(\langle p', \lambda'|\bar{\psi}(0)\gamma_i\lambda^\chi\psi(0)|p, \lambda\rangle\sigma_k\right), \tag{4}$$

where σ_j are the Pauli spin matrices. The $|\lambda\rangle$ is the corresponding spin state of the nucleon.

In SU(3) flavor the nucleon EMFFs are expressed in terms of the triplet and octet vector form factors:

$$G_{E,M}^N(Q^2) = \frac{1}{2}\left(G_{E,M}^3 + \frac{1}{\sqrt{3}}G_{E,M}^8\right), \tag{5}$$

while in flavor SU(2) they are written as

$$G_{E,M}^N(Q^2) = \frac{1}{2}\left(\frac{1}{3}G_{E,M}^0 + G_{E,M}^3\right). \tag{6}$$

Although the same notation is used for the form factors, it will always follow from the context of which flavor case is being addressed.

The matrix elements given in Eq. (4) can be evaluated both in the SU(2) and SU(3) flavor χQSMs. The model starts from the following low-energy effective partition function in Euclidean space:

$$\mathcal{Z}_{\chi\mathrm{QSM}} = \int \mathcal{D}\psi\mathcal{D}\psi^\dagger\mathcal{D}U \exp\left[-\int d^4x\Psi^\dagger iD(U)\Psi\right]$$

$$= \int \mathcal{D}U \exp(-S_{\mathrm{eff}}[U]), \tag{7}$$

where ψ and U denote the quark and pseudo-Goldstone boson fields, respectively. After integrating over the quark fields, the effective chiral action S_{eff} is given by

$$S_{\mathrm{eff}}(U) = -N_c\mathrm{Tr}\ln iD(U), \tag{8}$$

where Tr represents the functional trace and N_c the number of colors.

The Dirac $D(U) = \gamma_4(i\partial - \hat{m} - MU^{\gamma_5})$ operator, depending on the flavor space, is given by

$$D_{\mathrm{SU(2)}}(U) = -i\partial_4 + h(U)$$
$$D_{\mathrm{SU(3)}}(U) = -i\partial_4 + h(U) - \gamma_4\delta m \tag{9}$$

since, as isospin symmetry is assumed in this work, $\hat{m} = \mathrm{diag}(\overline{m}, \overline{m}) = \overline{m}\mathbf{1}_2$ in SU(2) and $\hat{m} = \mathrm{diag}(\overline{m}, \overline{m}, m_{\mathrm{s}}) = \overline{m}\mathbf{1}_3 + \delta m$ in SU(3), where

$$\delta m = \frac{-\overline{m} + m_{\mathrm{s}}}{3}\mathbf{1}_3 + \frac{\overline{m} - m_{\mathrm{s}}}{\sqrt{3}}\lambda^8 = M_1\mathbf{1}_3 + M_8\lambda^8. \tag{10}$$

The mass term δm containing the strange current quark mass m_{s} will be treated as a perturbation.

The single-quark Hamiltonian $h(U)$ is expressed as

$$h(U) = i\gamma_4\gamma_i\partial_i - \gamma_4 M U^{\gamma_5} - \gamma_4\overline{m}, \tag{11}$$

where U^{γ_5} stands for the chiral field for which we assume Witten's embedding of the SU(2) soliton into SU(3):

$$U_{\mathrm{SU(3)}}^{\gamma_5} = \begin{pmatrix} U_{\mathrm{SU(2)}}^{\gamma_5} & 0 \\ 0 & 1 \end{pmatrix} \tag{12}$$

with the SU(2) pion field π^i as

$$U_{\mathrm{SU(2)}}^{\gamma_5} = \exp(i\gamma^5\tau^i\pi^i) = \frac{1 + \gamma^5}{2}U_{\mathrm{SU(2)}} + \frac{1 - \gamma^5}{2}U_{\mathrm{SU(2)}}^\dagger. \tag{13}$$

The integration over the pion field U in Eq. (7) can be performed by the saddle-point approximation in the large-N_c limit due to the N_c factor in Eq. (8). The SU(2) pion field U is written as the most symmetric hedgehog form:

$$U_{\mathrm{SU(2)}} = \exp[i\gamma_5\hat{\boldsymbol{n}} \cdot \boldsymbol{\tau}P(r)], \tag{14}$$

where $P(r)$ is the radial profile function of the soliton.

The χQSM nucleon state $|N(p, s)\rangle$ used in the computation of Eqs. (1) and (4) is defined in terms of an Ioffe-type current consisting of N_c quarks:

$$|N(p, s)\rangle = \lim_{x_4 \to -\infty} \frac{1}{\sqrt{\mathcal{Z}}} e^{ip_4x_4} \int d^3x\, e^{i\boldsymbol{p}\cdot\boldsymbol{x}} J_N^\dagger(x) |0\rangle \tag{15}$$

with the Ioffe-type nucleon current J_N defined as

$$J_N(x) = \frac{1}{N_c!}\Gamma_N^{b_1\cdots b_{N_c}}\, \varepsilon^{\beta_1\cdots\beta_{N_c}}\, \psi_{\beta_1 b_1}(x)\cdots\psi_{\beta_{N_c} b_{N_c}}(x). \tag{16}$$

Here, the matrix $\Gamma_N^{b_1\cdots b_{N_c}}$ carries the hypercharge Y, isospin I, I_3, and spin s, s_3 quantum numbers of the baryon and the b_i and β_i denote the spin–flavor and color indices, respectively.

After minimizing the action in Eq. (8), we derive an equation of motion that is solved self-consistently with respect to the function $P(r)$ in Eq. (14). The corresponding unique solution U_c is called the classical chiral soliton. The next step consists in quantizing the classical soliton. This can be achieved by quantizing the rotational and translational zero-modes of the soliton. The rotations and translations of the soliton are implemented by

$$U(\boldsymbol{x}, t) = A(t)U_c(\boldsymbol{x} - \boldsymbol{z}(t))A^\dagger(t), \tag{17}$$

where $A(t)$ denotes a time-dependent SU(3) matrix, related to the orientation of the soliton in coordinate and flavor spaces, and $z(t)$ stands for the time-dependent translation of the center of mass of the soliton in coordinate space. The rotational velocity of the soliton $\Omega(t)$ is defined as

$$\Omega = \frac{1}{i}A^\dagger \dot{A} = \frac{1}{2i}\mathrm{Tr}(A^\dagger \dot{A}\lambda^\alpha)\lambda^\alpha = \frac{1}{2}\Omega_\alpha \lambda^\alpha. \tag{18}$$

Treating $\Omega(t)$ and δm perturbatively with a slowly rotating soliton and small δm considered, we find the collective Hamiltonian, i.e., the Hamiltonian in the collective coordinates of position of the center of mass and the orientation of the soliton, which is given explicitly as

$$H_{\mathrm{coll}}^{\mathrm{SU(2)}} = M_c^{\mathrm{SU(2)}} + \frac{1}{2I_1^{\mathrm{SU(2)}}}\sum_{i=1}^{3}J_iJ_i \tag{19}$$

in SU(2) and as

$$H_{\mathrm{coll}}^{\mathrm{SU(3)}} = H_{\mathrm{sym}} + H_{\mathrm{sb}} \tag{20}$$

$$H_{\mathrm{sym}} = M_c + \frac{1}{2I_1}\sum_{i=1}^{3}J_iJ_i + \frac{1}{2I_2}\sum_{a=4}^{7}J_aJ_a, \tag{21}$$

$$H_{\mathrm{sb}} = \frac{1}{m}M_1\Sigma_{SU(2)} + \alpha D_{88}^{(8)}(A) + \beta Y + \frac{\gamma}{\sqrt{3}}D_{8i}^{(8)}(A)J_i \tag{22}$$

in SU(3). M_c is the classical mass of the state, the parameters I are inertia parameters, Y is the hypercharge, $\Sigma_{SU(2)}$ is the pion–nucleon sigma term, the J are the angular momentum operators and $D^{(8)}$ are the SU(3) Wigner D functions. It is obvious that the strange quark in flavor SU(3) leads to a more involved analysis, particularly to the symmetry breaking contributions.

Within the collective quantization procedure the nucleon states given in Eq. (15) will be mapped to collective rotational functions carrying the state quantum numbers. In flavor SU(2) these functions are the eigenfunctions of the SU(2) symmetrical Hamiltonian, i.e., the Wigner D functions given as

$$\Psi_{JJ_3TT_3}(A) = \langle A|N(JJ_3;\ TT_3)\rangle$$

$$= (-1)^{T+T_3}\sqrt{2T+1}D_{-T_3,J_3}^{T=J}(A). \tag{23}$$

In flavor SU(3) the eigenfunctions of the SU(3) symmetric part of the Hamiltonian turn out to be the SU(3) Wigner D functions

$$\Psi_{Y;JJ_3;TT_3}^n(A) = \langle A|N(Y;\ JJ_3;\ TT_3)\rangle$$

$$= \sqrt{\dim n}(-1)^{-1/2+J_3}D_{T,T_3,Y;J,J_3,-1}^{(n)*}(A). \tag{24}$$

In contrast to the SU(2) case, the nucleon state is no longer a pure octet state but is a mixed state with those in higher representations arising from flavor SU(3) symmetry breaking, i.e.,

$$|N(Y;JJ_3;TT_3)\rangle = |8_{1/2}\ (Y;JJ_3;TT_3)\rangle$$

$$+ c_{\overline{10}}\sqrt{5}|\overline{10}_{1/2}\ (Y;JJ_3;TT_3)\rangle + c_{27}\sqrt{6}|27_{1/2}\ (Y;JJ_3;TT_3)\rangle, \tag{25}$$

where $c_{\overline{10}}$ and c_{27} denote the mixing parameters. These parameters, as well as the α, β, and γ in Eq. (22), may be found in Refs. [46,48].

A detailed formalism for the zero-mode quantization can be found in Refs. [46,48]. In addition, Ref. [53] offers a detailed description as to how the form factors can be obtained numerically. We briefly summarize it here before we discuss the numerical results. The parameters existing in the model are the constituent quark mass M, the current quark mass $\overline{m}$, the strange current quark mass m_{s}, and the cutoff mass Λ of the proper-time regularization. However, not all of them are free parameters but can be fixed in the mesonic sector without any ambiguity. In fact, this is a merit of the χQSM in which mesons and baryons can be treated on an equal footing. For a given M the regularization cutoff parameter Λ and the current quark mass $\overline{m}$ in the Lagrangian are fixed to the pion decay constant $f_\pi = 93$ MeV and the physical pion mass $m_\pi = 140$ MeV, respectively. The strange current quark mass is taken to be $m_{\mathrm{s}} = 180$ MeV, which approximately reproduces the kaon mass. Though the constituent quark mass M can be regarded as a free parameter, it is also more or less fixed. The experimental proton electric charge radius is best reproduced in the χQSM with the constituent quark mass $M = 420$ MeV. Moreover, the value of 420 MeV is known to yield the best fit to many baryonic observables [48]. Thus, all the numerical results in the present work are obtained with this value of M.

All the results presented in the following were computed completely within the model, in the same level of approximation, to maintain consistency. In particular, magnetization observables are presented not in terms of the physical nuclear magneton but, instead, in terms of the model nuclear magneton, i.e., defined as the model value for the nucleon mass, which, at the level of approximation used in this work, is

$$M_N = 1250 \text{ MeV}. \tag{26}$$

We want to mention that the ratio between the model nuclear magneton and the physical one is the same as that between the value of M_N in Eq. (26) and the physical nucleon mass.

To address the properties of the baryon octet immediately implies flavor structures of the SU(3) baryons. However, it simultaneously indicates the question of how accurate the χQSM description of the strangeness content of the nucleon is and its implications for the EMFF. Such a question could easily be answered if one had precise experimental data on the strange EMFF. The present study may give some clues to the answer for that question in the light of the recent phenomenological data [23,24].

3. Sachs form factors

The Sachs EM form factors [65,66] are the most common form to encompass information about the electromagnetic structure of the nucleon. On the one hand, these form factors make it possible to express the cross section for elastic electron–proton scattering in the one-photon exchange approximation, without mixed terms ($G_E G_M$) in a form suitable for the separation of the electric and magnetic form factors. That is not the case when the cross section is expressed in terms of the Dirac and Pauli form factors (1), where mixed terms ($F_1 F_2$) occur. Even with the more recent polarization transfer methods [67], the measured ratio between the longitudinal and transverse polarization components is expressed in terms of the Sachs form-factor ratio $\mu G_E / G_M$.

On the other hand, the Sachs form factors have a merit that in the Breit frame they may be apparently interpreted as the Fourier transform of the charge and magnetization distributions inside a nucleon. This comes from the fact that in the Breit frame the proton does not exchange energy with the
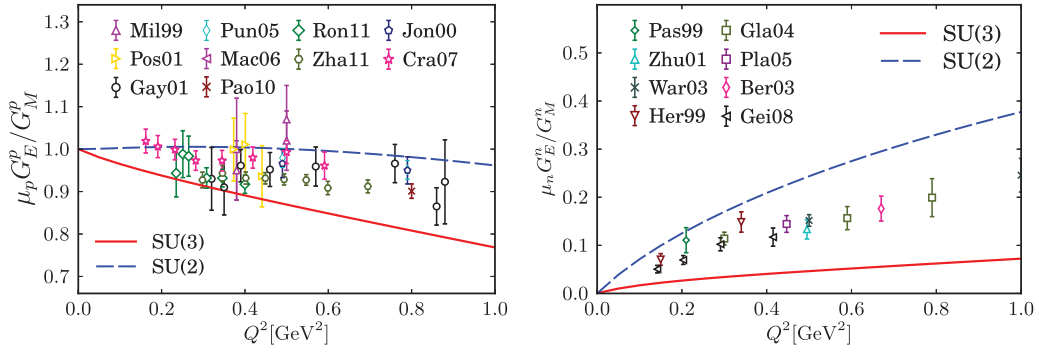
Fig. 1. The ratio of the proton magnetic FF to the electric FF: $\mu G_E/G_M$ in the left panel. The experimental data are taken from Mil99 [71], Pos01 [72], Gay01 [2], Mac06 [73], Pao10 [74], Ron11 [7], Zha11 [8], Jon06 [76], Jon00 [1], Cra07 [77]. The neutron $\mu G_E/G_M$ ratio in the right panel compared to the data from recent experiments: Pas99 [78], Zhu01 [79], War03 [80], Gei08 [81], Her99 [82], Gla04 [83], Pla05 [84], Ber03 [85]. The solid curve depicts the result from the SU(3) χQSM; the dashed one that from the SU(2) model.

virtual photon with momentum $(0, \boldsymbol{q})$. At a specific space-like $Q^2 = -\boldsymbol{q}^2 < 0$ invariant momentum transfer, the time and space components of the electromagnetic current, associated with the electric and magnetic form factors respectively, resemble the classical non-relativistic current density. Hence the Sachs EM form factors are directly related to the charge and magnetization distributions by the Fourier transform. However, these relations are supposedly non-relativistic in nature due to the Q^2 dependence of the Breit frame. Both the preceding features of the Sachs form factors are currently under scrutiny, as mentioned in the introduction. Discrepancies in the experimental results from the elastic *ep* cross section and polarization transfer studies called for the inclusion of new aspects of elastic electron–proton scattering, such as two-photon exchange [18]. The connection between form factors and densities, even apart from the non-relativistic limitation, has also been revised on general grounds [68,69].

In the left panel of Fig. 1, the results of the ratio of the proton magnetic FF to the electric FF are depicted in comparison with the experimental data from the recoil polarization experiments $p(\vec{e}, e'\vec{p})$ [1,2,5,7,8,71–75] and the experiments with a polarized target $\vec{p}(\vec{e}, e'p)$ [76,77]. The SU(2) results can describe the general tendency of the data very well, whereas those of SU(3) seem slightly underestimated, as Q^2 increases. The right panel of Fig. 1 plots the results for the ratio $\mu_n G_E^n/G_M^n$, compared with the experimental data taken from $\vec{d}(\vec{e}, en)p$ [78–81] and from $d(\vec{e}, e'\vec{n})p$ [82–84] and $^3\mathrm{He}(\vec{e}, e'n)$ scatterings [85]. We observe that the experimental data lie between the SU(2) and SU(3) results. The general tendency of the present results is in line with the experimental data: $\mu_p G_E^p/G_M^p$ falls off slowly as Q^2 increases, while $\mu_n G_E^n/G_M^n$ increases systematically as a function of Q^2. As shown in the right panel of Fig. 1, the SU(3) results for the neutron are rather different from those in SU(2), the reason stemming, at least partially, from the strange-quark contribution to the neutron electric FF. Because of the embedding of the SU(2) soliton into SU(3) as shown in Eq. (12), the contribution of the strange quark has the same asymptotic behavior of the nonstrange quarks. The effects due to different asymptotic tails were discussed in Ref. [86] in the context of the strange vector FFs of the nucleon. Thus, in a sense, a true answer may be found between the SU(2) and the SU(3) results.

In order to decompose the proton EMFFs into flavor ones, we need to compute the singlet vector form factors of the proton. Then, we are able to express the flavor-decomposed EMFFs of the proton in terms of the singlet, triplet, and octet FFs of the proton:

Table 1. The flavor-decomposed magnetic moments are defined as $\mu_q = G_M^q(0)$ and are presented in unit of the model nuclear magneton μ_N.

	μ_u	μ_d	μ_s
SU(3)	3.22	−0.73	0.10
SU(2)	3.46	−0.95	
Ref. [24]	3.67	−1.03	

$$G_{E,M}^u(Q^2) = \frac{1}{2}\left(\frac{2}{3}G_{E,M}^{(0)}(Q^2) + G_{E,M}^{(3)}(Q^2) + \frac{1}{\sqrt{3}}G_{E,M}^{(8)}(Q^2)\right),$$

$$G_{E,M}^d(Q^2) = \frac{1}{2}\left(\frac{2}{3}G_{E,M}^{(0)}(Q^2) - G_{E,M}^{(3)}(Q^2) + \frac{1}{\sqrt{3}}G_{E,M}^{(8)}(Q^2)\right),$$

$$G_{E,M}^s(Q^2) = \frac{1}{3}\left(G_{E,M}^{(0)}(Q^2) - \sqrt{3}G_{E,M}^{(8)}(Q^2)\right), \tag{27}$$

where we have suppressed the corresponding quark charge. The normalizations at $Q^2 = 0$ for the proton obey $G_E^u(0) = 2$, $G_E^d(0) = 1$, and $G_E^s(0) = 0$. The flavor-decomposed magnetic moments are listed in Table 1 in units of the model nuclear magneton, i.e., defined with the model nucleon mass.

The Sachs FFs for the different quark flavors are presented in Fig. 2, normalized by the dipole parametrization defined as

$$G_D(Q^2) = \frac{1}{\left(1 + \frac{Q^2}{\Lambda_D^2}\right)^2}, \qquad \Lambda_D^2 = 0.71\,\text{GeV}^2 \tag{28}$$

in comparison with the phenomenological data taken from Ref. [24] (including the online supplemental material), whose normalizations at $Q^2 = 0$ are given as $G_M^u = 3.67\,\mu_N$ and $G_M^d = -1.03\,\mu_N$. The up and down electric FFs are more or less well reproduced. On the one hand, the up magnetic FF deviates from the data, as Q^2 increases, but the Q^2 dependence of the down magnetic FF shows a similar tendency to the data but the results seem a bit overestimated. Since there are no corresponding experimental data yet for the strange EMFFs, the lower panel of Fig. 2 shows the predictions of the present model for the strange EMFFs.

4. Dirac and Pauli form factors

The Dirac (F_1) and Pauli (F_2) FFs are expressed in terms of the Sachs EMFFs inverting Eq. (3), i.e.,

$$F_1(Q^2) = \frac{G_E + \tau G_M}{1 + \tau}$$

$$F_2(Q^2) = \frac{G_M - G_E}{1 + \tau}, \tag{29}$$

where τ is given by

$$\tau = Q^2/(4M^2). \tag{30}$$

As mentioned in the introduction, pQCD with factorization schemes [20] predicts that the nucleon Dirac FFs scale with $1/Q^4$. It indicates that $Q^4 F_1(Q^2)$ becomes asymptotically constant. Thus,
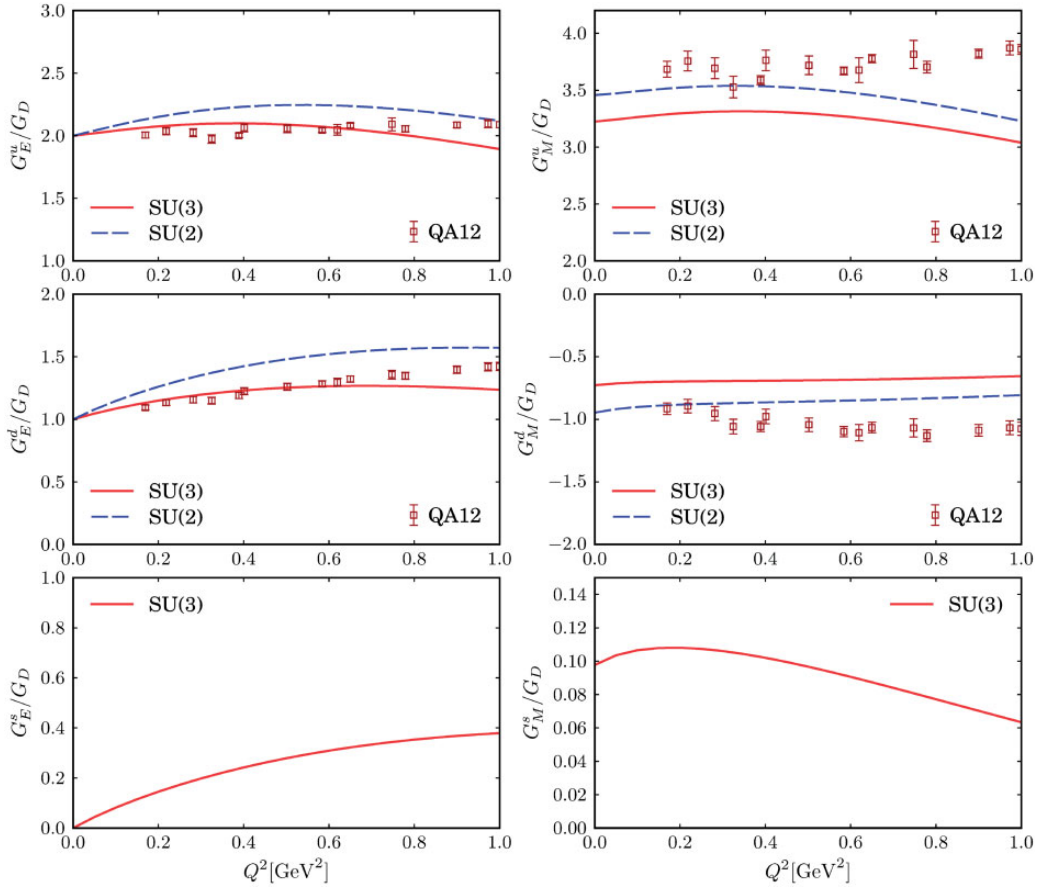
Fig. 2. Ratios of the nucleon Sachs flavor FFs to the dipole parametrizations (Eq. (28)). The u quark FFs are shown in the upper panel, the d quark FFs in the middle panel, and the strange ones in the lower panel. The phenomenological data are taken from Ref. [24] (including the online supplemental material) (QA12). Notations are the same as in Fig. 1.

$Q^4 F_1(Q^2)$ is a more interesting quantity than F_1 itself. Figure 3 shows the results for the nucleon Dirac FFs with Q^4 factor in comparison with the experimental data [23,24,26] (including the online supplemental material for Ref. [24]). The Q^2 dependence of $Q^4 F_1^p(Q^2)$ is well explained within the SU(2) model, while that from the corresponding SU(3) model seems slightly underestimated, especially as Q^2 increases. However, as for $Q^4 F_1^n(Q^2)$, the result of the SU(3) model describes the data well, whereas the SU(2) F_1 turns out positive. As shown in the lower panel of Fig. 3, the results of $Q^6 F_2(Q^2)/\kappa$ for both the proton and the neutron are in good agreement with the experimental data. However, due to the momentum transfer range, the scaling behavior is not clear.

The flavor-decomposed Dirac (F_1^q) and Pauli (F_2^q) FFs are expressed as

$$F_{1,2}^u = 2F_{1,2}^p + F_{1,2}^n + F_{1,2}^s,$$
$$F_{1,2}^d = F_{1,2}^p + 2F_{1,2}^n + F_{1,2}^s \tag{31}$$

in flavor SU(3). In flavor SU(2), the up and down Dirac and Pauli FFs are simply written in terms of the corresponding proton and neutron FFs:

$$F_{1,2}^u = 2F_{1,2}^p + F_{1,2}^n,$$
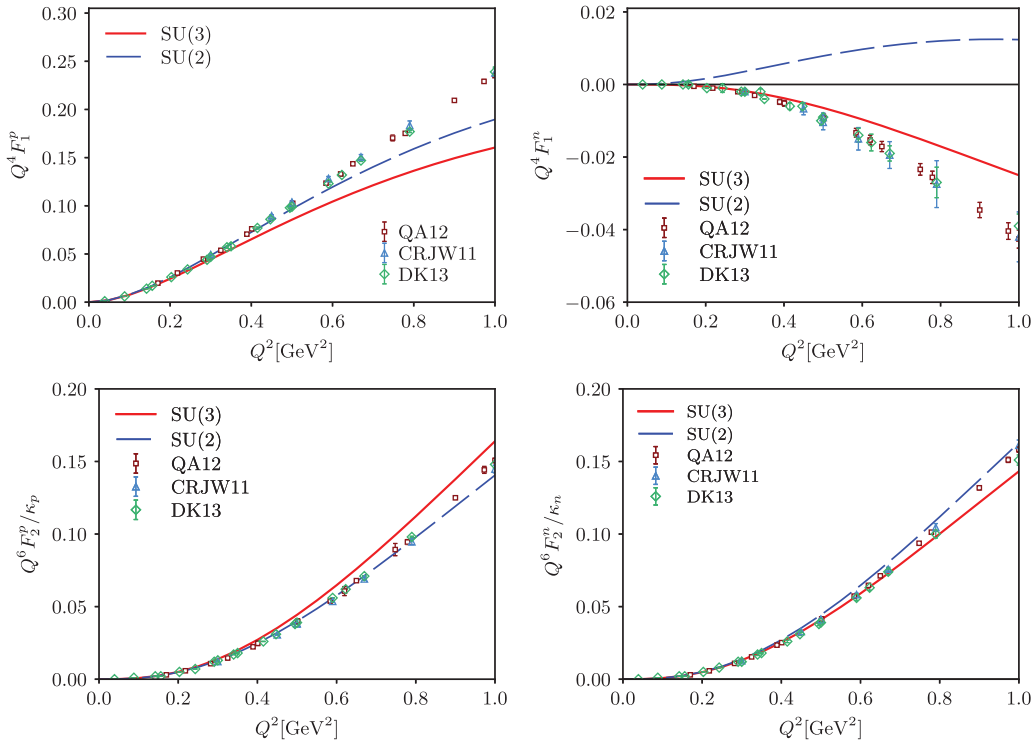$$F_{1,2}^d = F_{1,2}^p + 2F_{1,2}^n. \tag{32}$$

Fig. 3. Dirac FFs F_1 of the proton and the neutron, scaled with Q^4 in the upper panel and the Pauli FFs scaled with $Q^6/\kappa_{p(n)}$ in the lower panel. The experimental data are taken from Refs. [23] (CRJW11), [24] (including the online supplemental material) (QA12), and [26] (DK13). Notations are the same as in Fig. 1.

Table 2. Anomalous magnetic moments $\kappa = F_2(0)$ for the proton and the nucleon. The flavor-decomposed anomalous magnetic moments are also presented. Exp. & Phen. denote the experimental data on the proton and the neutron anomalous magnetic moments, and the empirical data on the flavor-decomposed ones.

	κ_p	κ_n	κ_u	κ_d	κ_s
SU(3)	1.36	-1.59	1.22	-1.73	0.10
SU(2)	1.62	-1.78	1.46	-1.95	
Exp. & Phen.	1.793	-1.913	1.673	-2.033	

Note, however, that $F_{1,2}^{u,d}$ do not turn out the same in SU(3) and SU(2) just by neglecting $F_{1,2}^s$ since the flavor groups are different.

In Fig. 4, we show the results of $Q^4 F_1^q$ and $Q^4 F_2^q/\kappa^q$ for the up (u), down (d), and strange (s) quarks, respectively. $Q^4 F_1^u$ shows a stronger Q^2 dependence than that of $Q^4 F_1^d$ while $Q^4 F_2^u$ exhibits a weaker Q^2 dependence than that of $Q^4 F_2^d$. The present results for both the up and down quarks describe the data very well as in the case of the proton and neutron FFs (see Fig. 3). Again, we predict $Q^4 F_1^s$ and $Q^4 F_2^s$.

At $Q^2 = 0$ the Dirac and FFs are respectively reduced to $F_1^p(0) = 1$, $F_1^n(0) = 0$, and $F_2^{p(n)}(0) = \kappa_{p(n)}$ with the corresponding anomalous magnetic moment $\kappa_{p(n)}$ (see Table 2). For the flavor-decomposed Dirac FFs, with our normalization $F_1^u(0) = 2$, $F_1^d(0) = 1$, and $F_1^s(0) = 0$.
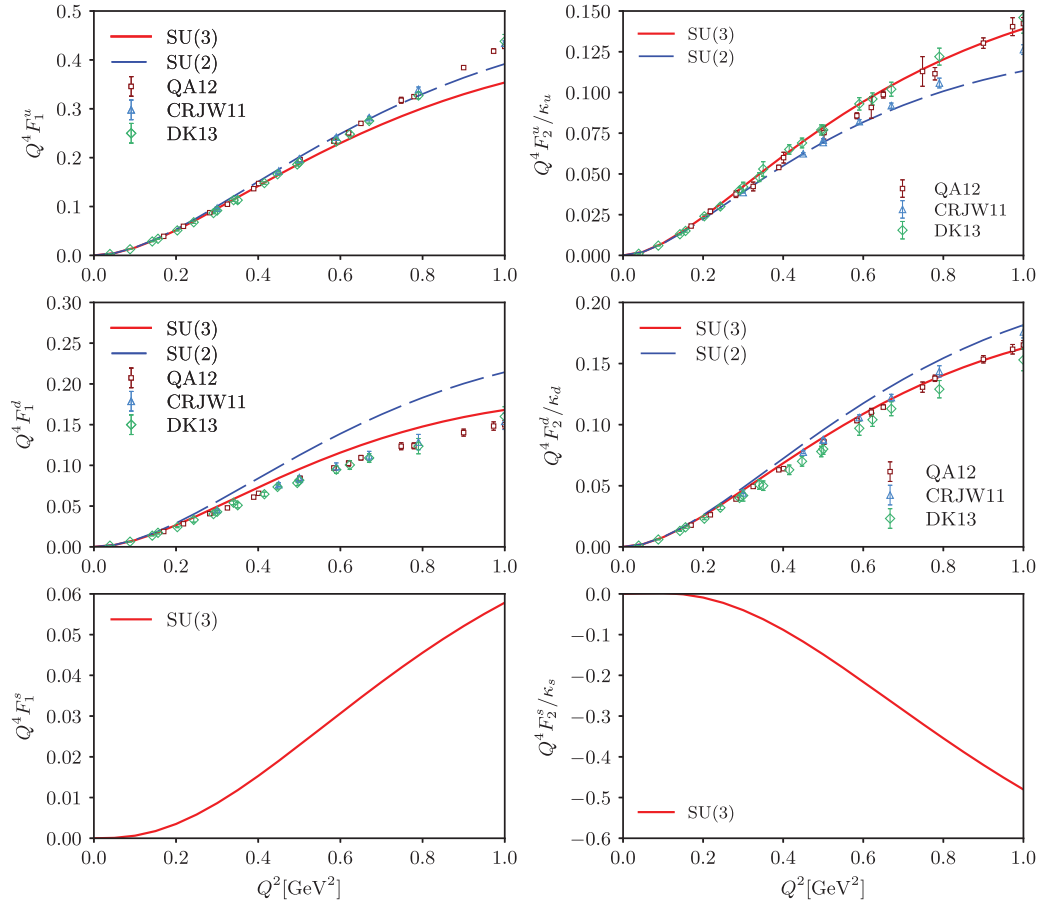
Fig. 4. The flavor-decomposed Dirac and Pauli FFs weighted by Q^4: The up FFs are shown in the upper panel, the down ones in the middle panel, and the strange FFs in the lower panel. The experimental data are taken from Refs. [23] (CRJW11), [24] (including the online supplemental material) (QA12), and [26] (DK13). Notations are the same as in Fig. 1.

5. Transverse charge densities

We are now in a position to discuss the quark transverse charge densities inside both unpolarized and polarized nucleons. The traditional charge and magnetization densities in the Breit framework are defined ambiguously because of the Lorentz contraction of the nucleon in its moving direction [87,88]. To avoid this ambiguity one can define the quark charge densities in the transverse plane. Then, they provide essential information on how the charges and magnetizations of the quarks are distributed in the transverse plane. When the nucleon is unpolarized, the quark transverse charge density is defined as the 2D Fourier transform of the nucleon Dirac FFs:

$$\rho_{\text{ch}}(b) = \frac{1}{(2\pi)^2} \int d^2q \, e^{i\boldsymbol{q}\cdot\boldsymbol{b}} F_1(Q^2) = \int_0^\infty \frac{dQ}{2\pi} Q J_0(Qb) F_1(Q^2), \tag{33}$$

where b denotes the impact parameter, i.e., the distance in the transverse plane to the place where the density is being probed, and J_0 is a cylindrical Bessel function of order zero [68,69]. Note that the Dirac FF at $Q^2 = 0$ and the anomalous magnetic moment can be rederived from the transverse charge and magnetization densities:

$$2\pi \int db \, b \, \rho_{\text{ch}}(b) = F_1(0), \qquad \pi \int db \, b \, \rho_{\text{m}}(b) = \kappa, \tag{34}$$
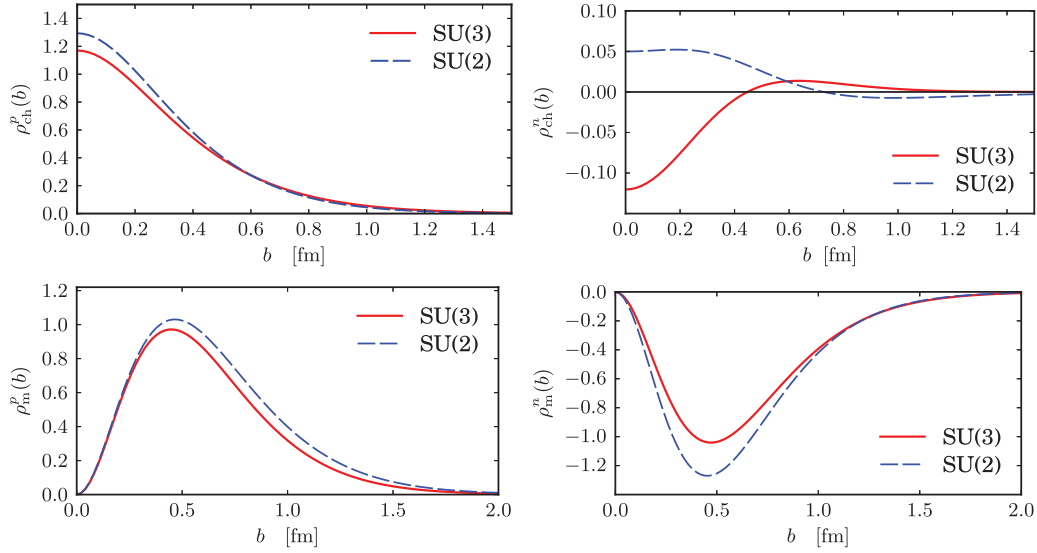
Fig. 5. Transverse charge densities inside a proton (upper left panel) and a neutron (upper right panel), and the transverse magnetization densities inside a proton (lower left panel) and a neutron (lower right panel). Notations are the same as in Fig. 1.

either for the nucleon or for each individual flavor, with the anomalous magnetization density in the transverse plane defined [69,70] by

$$\rho_{\mathrm{m}}(b) = b \int_0^\infty \frac{dQ}{2\pi} Q^2 J_1(Qb) F_2(Q^2). \tag{35}$$

By definition, Eqs. (33), (35) seem to imply the knowledge of Dirac and Pauli form factors over a wide range of Q^2 in order to obtain meaningful densities. This seems at odds with the fact that the present χCQSM FFs are obtained in low transferred momenta. However, it turns out that with the model form factors, the integrals in Eqs. (33), (35) are saturated in the range $Q^2 < 1.5$ $(\mathrm{GeV}/c)^2$, i.e., the computed densities do not change when the upper limit in the integrals is set at different values above 1.5 $(\mathrm{GeV}/c)^2$.

In the upper panel of Fig. 5, the transverse charge densities inside both a proton and a neutron are shown. The results of the transverse charge density from the SU(2) model are almost the same as those from the SU(3) model for the proton. However, it is very interesting to observe that the transverse charge density inside the neutron from the SU(2) model is opposite to that of the SU(3) one. As already found in Figs. 1 and 3, the SU(2) result is distinguished from the SU(3) one, mainly due to the effects of the strange quark. These are in fact surprising results, because the SU(3) result interprets the inner structure of the neutron totally differently from the SU(2) one: While the negative charge, which mainly comes from the down and strange quarks inside a neutron, is centered on the neutron according to the SU(3) χQSM, the SU(2) model suggests that the positive one is located in the center of the neutron. In Ref. [68], the transverse charge density of the neutron was computed, based on the parametrization of the experimental EMFFs, and was found to be negative in the center of the neutron, which is in line with the present result from the SU(3) model. To clarify this discrepancy between the SU(2) and SU(3) models, it might be essential to know the strangeness content of the neutron. We will discuss later each contribution of a quark with different flavor to the transverse charge density inside the neutron in more detail. Another interesting point in the transverse charge
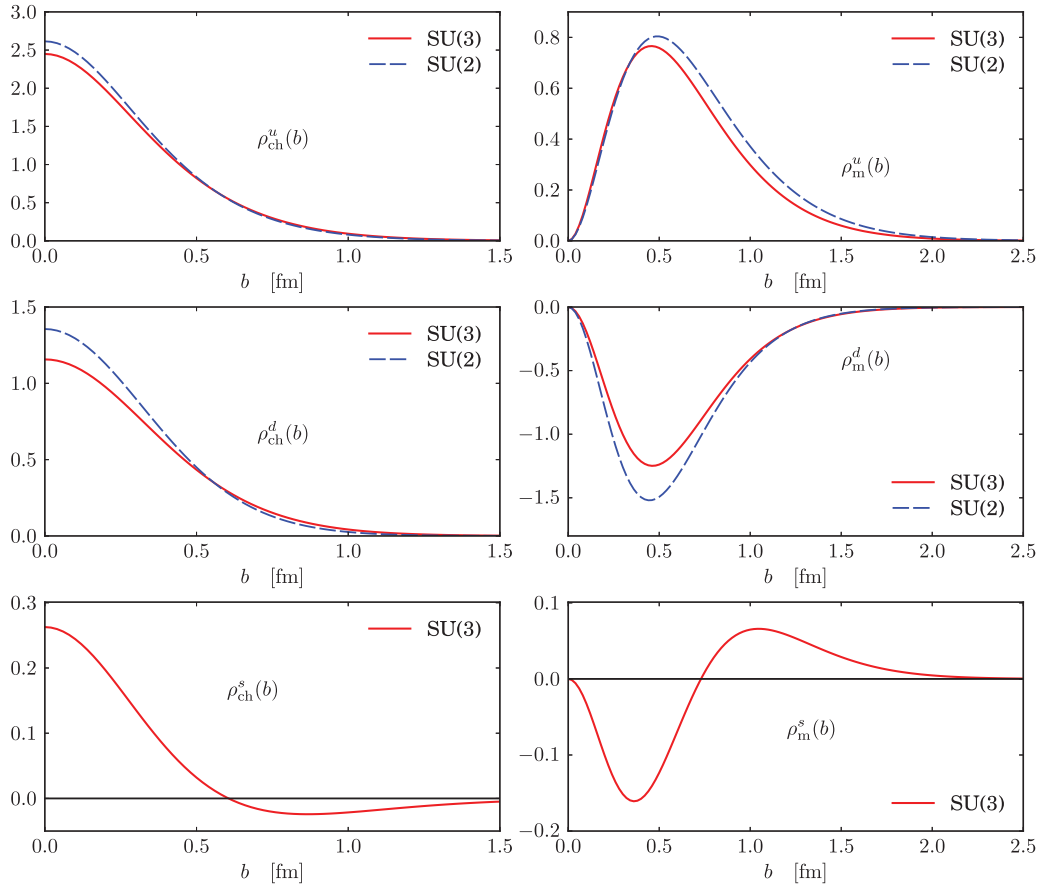
Fig. 6. Flavor-decomposed transverse charge and magnetization densities inside a proton. Those for the up quark are shown in the upper panel, the down ones in the middle panel, and the strange charge and magnetization densities in the lower panel. Notations are the same as in Fig. 1.

density inside a neutron is that it turns positive as b increases. The reason will soon be clear when we discuss the flavor-decomposed transverse charge densities.

The lower panel of Fig. 5 plots the transverse magnetization densities inside both a proton and a neutron. The results from the SU(2) model are similar to those from the SU(3) model. As expected from their values of the anomalous magnetic moments, the transverse magnetization densities inside a proton are positive but those inside a neutron turn out to be negative. We will soon observe that the up quark and the down quark contribute oppositely to the magnetization, which explains the results of the transverse magnetization densities inside a proton and a neutron.

In Fig. 6, the transverse charge and magnetization densities are depicted for each flavor, in the left panel and the right panel, respectively. The results of the transverse densities in Fig. 6 do not include the charges for each flavor. The charge densities for the up and down quarks look similar to the proton one shown in Fig. 5 and the SU(2) results are generally larger in the center region but fall off faster than the SU(3) ones. The strange-quark case shows interesting features. While the charge density is found to be positive in the inner region, it becomes negative as b increases. Note that the down quark inside a nucleon is more magnetized than the up quark but was directed opposite to the up quark, which results in the negative larger value of the anomalous magnetic moment for the down quark than for the up quark (see Table 2). The strange transverse magnetization densities look very different from those for the up and down quarks: In the inner part of the nucleon, the strange quark is

negatively magnetized. As b increases, the strange magnetization density turns positive. As a result, the strange anomalous magnetic moment turns out to be small but positive: $\kappa_s = 0.10$ (see Table 2).

As discussed, the SU(3) transverse charge density was very different from the SU(2) one. We can understand the reason for this from the results of the flavor-decomposed transverse charge densities. The transverse charge densities inside a proton and a neutron can be respectively expressed in terms of the flavor-decomposed ones:

$$\rho_{\text{ch}}^{p} = \frac{1}{3}(2\,\rho_{\text{ch}}^{u} - \rho_{\text{ch}}^{d} - \rho_{\text{ch}}^{s}),$$

$$\rho_{\text{ch}}^{n} = \frac{1}{3}(2\,\rho_{\text{ch}}^{d} - \rho_{\text{ch}}^{u} - \rho_{\text{ch}}^{s}). \tag{36}$$

Since ρ_{ch}^{u} governs the transverse charge density inside a proton (ρ_{ch}^{p}) as shown in Fig. 6, ρ_{ch}^{s} has almost negligible effects on it. However, when it comes to ρ_{ch}^{n}, $2\,\rho_{\text{ch}}^{d}$ and ρ_{ch}^{u} in Eq. (36) almost cancel each other out, which results in a small amount of the negative density. In addition, ρ_{ch}^{s} contributes negatively to ρ_{ch}^{n}, which finally leads to the negative value of ρ_{ch}^{n} in the centered region, as shown in Fig. 5. In the case of the SU(2) model, ρ_{ch}^{d} turns out to be larger than that from the SU(3) model, so that ρ_{ch}^{n} becomes positive but tiny. Thus, the strange transverse charge density, though it is small, plays an essential role in explaining the negative value of ρ_{ch}^{n} in the center of the neutron within the framework of the χQSM. Moreover, the strange transverse charge density turns positive as b increases. This partly explains why ρ_{ch}^{n} becomes negative at higher b.

When the nucleon is transversely polarized along the x axis, which can be described by the transverse spin operator of the nucleon $\boldsymbol{S}_{\perp} = \cos\phi_S \hat{\boldsymbol{e}}_x + \sin\phi_S \hat{\boldsymbol{e}}_y$, the transverse charge density inside a transversely polarized nucleon is expressed [89] as

$$\rho_{\text{T}}(\boldsymbol{b}) = \rho_{\text{ch}}(b) - \sin(\phi_b - \phi_S)\frac{1}{2M_N b}\rho_{\text{m}}(b), \tag{37}$$

where $\rho_{\text{m}}(b)$ is given in Eq. (35). The position vector $\boldsymbol{b}$ from the center of the nucleon in the transverse plane is denoted as $\boldsymbol{b} = b(\cos\phi_b \hat{\boldsymbol{e}}_x + \sin\phi_b \hat{\boldsymbol{e}}_y)$. The x axis is taken as the polarization direction of the nucleon, i.e., $\phi_S = 0$. In the upper-left panel of Fig. 7, we plot the transverse charge densities inside a transversely polarized proton. It is shown that the charge density for the transversely polarized proton is distorted in the negative y direction. As discussed in Refs. [88,89], the transverse polarization of the nucleon in the x axis induces the electric dipole moment along the negative y direction, which is a well known relativistic effect. In the case of the neutron, the situation is even more dramatic. As shown in the upper-right panel of Fig. 5, the negative charge is located at the center of the neutron with the positive charge surrounding it. However, when the neutron is transversely polarized along the x axis, the negative charge is shifted to the negative y direction but the positive one is moved to the positive y direction. This comes from the fact that the neutron anomalous magnetic moment is negative, which yields an induced electric dipole moment along the positive y axis, as pointed out by Ref. [89].

It is very instructive to examine the transverse charge densities inside the transversely polarized nucleon for each flavor, since they reveal with more detail the inner structure of the nucleon. Figure 8 illustrates them. The up transverse charge density inside the transversely polarized nucleon, ρ_{T}^{u}, is shown to be shifted to the negative direction, while that for the down quark is more distorted upwards. This is natural, since the up and down quarks have positive and negative charges, respectively. However, it is remarkable to see that the down quark is influenced more strongly due to the transverse
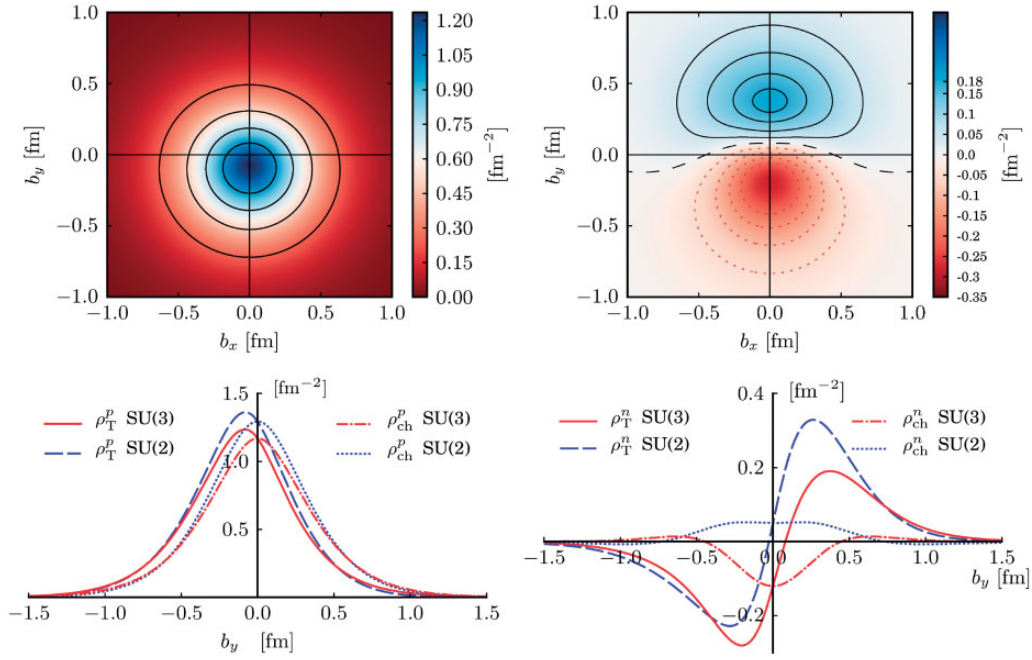
Fig. 7. Transverse charge densities inside a transversely polarized nucleon. The upper-left and upper-right panels show the transverse charge densities inside a proton and a neutron, respectively, being polarized along the x axis. The lower panel depicts the corresponding transverse charge densities on the y axis with b_x fixed ($b_x = 0$): The solid curve corresponds to the results of the transverse charge densities inside transversely polarized nucleons from the SU(3) model; the dashed curve to those from the SU(2) model. The dotted and dash-dotted curves represent the SU(2) and SU(3) results for the transverse charge densities inside unpolarized nucleons, respectively.
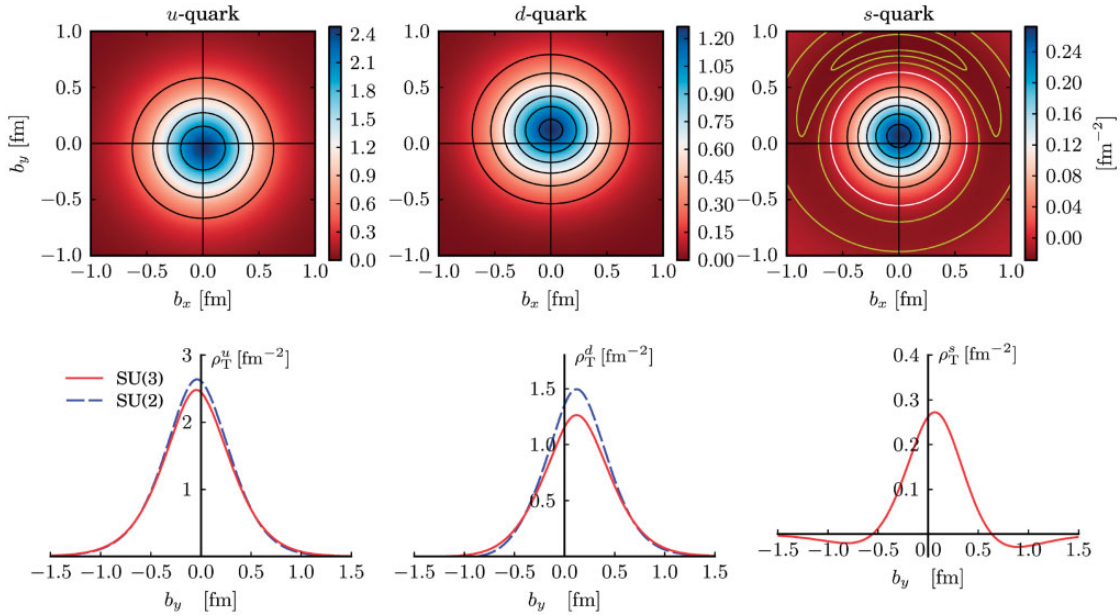

Fig. 8. Flavor-decomposed transverse charge densities inside a transversely polarized nucleon. The upper-left, upper-middle, and upper-right panels show the up, down, and strange transverse charge densities inside a proton and a neutron, respectively, being polarized along the x axis. The lower panel depicts the corresponding transverse charge densities in the y axis with b_x fixed ($b_x = 0$). Notations are the same as in Fig. 1.

polarization of the nucleon. ρ_T^s is even more interesting. As discussed previously, the strange anomalous magnetic moment is $\kappa_s = +0.10$, which would induce the negative electric dipole moment along the negative b_y. However, the situation turns out to be more complicated. As shown in the right panel of Fig. 8, ρ_T^s is shifted to the positive b_y and turns negative starting from $b_y \approx 0.7$ fm. In order to understand this surprising result, we need to reexamine the transverse magnetization density for the strange quark, which has been presented in Fig. 6. The strange magnetization density is negative in the inner part of the nucleon and then it becomes positive from $b \approx 0.7$ fm. Thus, the electric dipole moment is correspondingly induced along the positive y direction in the centered region, and then it becomes negative from $b \approx 0.7$ fm, as shown in the right panel of Fig. 8.

6.   Summary and conclusion

In the present work, we aimed to investigate the electromagnetic properties of the nucleon, based on the SU(2) and SU(3) chiral quark–soliton models with symmetry-preserving quantization employed. We considered the rotational $1/N_c$ corrections and the first-order m_s corrections. It should be stressed at this point that no free parameters were used in this work. The only model parameter to be constrained in the baryon sector, namely, the constituent quark mass, was taken from previous studies with various observables.

We first presented the results of the ratio of the magnetic form factor to the electric form factor of the proton. It was shown that the results from the SU(2) chiral quark–soliton model described the experimental data very well, whereas those of SU(3) seemed slightly underestimated in higher Q^2. The general tendency of the present results was in agreement with the experimental data. As for the neutron, the SU(3) results turned out to be rather different from those in SU(2), which arose from the strange-quark contribution to the neutron electric form factor. In particular, the neutron electric form factor is rather sensitive to the tail of the soliton. We then discussed that the up and down electric form factors normalized by the dipole parametrization were well reproduced in comparison with the data. As for the magnetic form factors, they deviate from the experimental data as Q^2 increases but the general behavior of the form factors is in line with the experimental data, which indicates that the Q^2 dependence is well explained. We presented the prediction of the strange form factors normalized by the dipole form factor.

The Dirac and Pauli form factors were predicted to be asymptotically proportional to $1/Q^4$ and $1/Q^6$ respectively in perturbative QCD. Thus, we studied $Q^4 F_1(Q^2)$ and $Q^6 F_2(Q^2)$ in order to compare their Q^2 dependence with the experimental data. We found that the present SU(2) model explained $Q^4 F_1^p(Q^2)$ well whereas the result from the SU(3) model becomes underestimated at higher Q^2. Both the SU(2) and SU(3) results for $Q^6 F_2^{p,n}(Q^2)/\kappa_{p,n}$ described the experimental data very well. On the other hand, the SU(2) result for $Q^4 F_1^n$ is in conflict with the data, but that from the SU(3) model is in agreement with the data except for the higher Q^2 region. Again, this discrepancy can be understood by the sensitivity of the neutron electric form factor to the soliton tail. The results for the flavor-decomposed $Q^4 F_1(Q^2)$ and $Q^6 F_2(Q^2)$ were shown to be generally in good agreement with the corresponding values from the experimental data.

Having performed the 2D Fourier transform of the nucleon electromagnetic form factors, we were able to produce the charge densities in the transverse plane inside a proton. As expected, both the SU(2) and SU(3) transverse charge densities were positive in the proton. However, as for the neutron case, the result from SU(2) was opposite to that from SU(3): the negative charge was located in the center of the neutron while the positive one was distributed in the outer part within the SU(3) chiral quark–soliton model; it was the other way around in the SU(2) model. The explanation for this

comes from the decomposed-flavor transverse charge densities in the SU(3) model. In particular, the component of the strange quark played an essential role in spite of the smallness of its magnitude. Since the up-quark component mainly contributed to the transverse charge density inside a proton, the strange transverse charge density was almost negligible. On the other hand, the up- and down-quark contributions were nearly canceled out in such a way that the negative charge remained in the center of the neutron with small magnitude. Then the contribution of the strange quark came into play, so that the transverse charge densities inside a neutron finally became negative in the center.

When the proton was polarized along the positive x direction, the corresponding transverse charge density was shifted to the negative y direction, which indicated that the electric dipole moment was induced along the negative y direction. This is just a well known relativistic effect in electrodynamics. In the case of the neutron polarized along the x axis, the negative charge was moved to the negative y direction but the positive one was forced to the positive y axis. This implies that the neutron anomalous magnetic moment is negative, which induces an electric dipole moment along the positive y axis. We also decomposed the transverse charge densities inside the polarized nucleon for each flavor: the up transverse charge density for the nucleon transversely polarized along the positive x axis was found to be shifted to the negative direction, while that of the down quark was more distorted upwards. Since the up and down quarks have positive and negative charges, respectively, one can easily understand these features. However, the down quark was found to be affected more strongly due to the transverse polarization of the nucleon. The strange charge density inside the transversely polarized nucleon was shifted to the positive b_y and turned out to be negative in the outer region. This unexpected behavior of the strange charge density for the transversely polarized nucleon was explained in terms of the strange magnetization density.

Since the transverse charge densities inside unpolarized and polarized nucleons pave a novel way for understanding the internal structure of the nucleon, it is interesting to investigate them for other baryons such as the Δ isobar and hyperons. The transverse charge densities are directly connected to the generalized parton distributions, integrations of which over parton momentum fractions yield form factors and consequently the spatial distribution of partons in the transverse plane. Moreover, the transverse charge densities for transition form factors provide a new aspect of understanding the inner structure of baryons. For example, as already studied in Ref. [89], they exhibit explicitly multipole structures of the transitions in the transverse plane. Thus, it is of great importance to examine the transverse charge densities for other baryons and for their transitions. Corresponding investigations are underway.

References

[1] M. K. Jones et al. [Jefferson Lab Hall A Collaboration], Phys. Rev. Lett. **84**, 1398 (2000) [arXiv:nucl-ex/9910005] [Search INSPIRE].

[2]   O. Gayou et al. [Jefferson Lab Hall A Collaboration], Phys. Rev. C **64**, 038202 (2001).

[3]   O. Gayou et al. [Jefferson Lab Hall A Collaboration], Phys. Rev. Lett. **88**, 092301 (2002) [arXiv:nucl-ex/0111010] [Search INSPIRE].

[4]   V. Punjabi et al. [Jefferson Lab Hall A Collaboration], Phys. Rev. C **71**, 055202 (2005); **71**, 069902 (2005) [erratum] [arXiv:nucl-ex/0501018] [Search INSPIRE].

[5]   A. J. R. Puckett et al., Phys. Rev. Lett. **104**, 242301 (2010) [arXiv:1005.3419 [nucl-ex]] [Search INSPIRE].

[6]   J. C. Bernauer et al. [A1 Collaboration], Phys. Rev. Lett. **105**, 242001 (2010) [arXiv:1007.5076 [nucl-ex]] [Search INSPIRE].

[7]   G. Ron et al. [Jefferson Lab Hall A Collaboration], Phys. Rev. C **84**, 055204 (2011) [arXiv:1103.5784 [nucl-ex]] [Search INSPIRE].

[8]   X. Zhan et al., Phys. Lett. B **705**, 59 (2011) [arXiv:1102.0318 [nucl-ex]] [Search INSPIRE].

[9]   C. E. Hyde-Wright and K. de Jager, Ann. Rev. Nucl. Part. Sci. **54**, 217 (2004) [arXiv:nucl-ex/0507001] [Search INSPIRE].

[10] J. Arrington, C. D. Roberts, and J. M. Zanotti, J. Phys. G: Nucl. Part. Phys **34**, S23 (2007) [arXiv:nucl-th/0611050] [Search INSPIRE].

[11] C. F. Perdrisat, V. Punjabi, and M. Vanderhaeghen, Prog. Part. Nucl. Phys. **59**, 694 (2007) [arXiv:hep-ph/0612014] [Search INSPIRE].

[12] M. Vanderhaeghen and T. Walcher, arXiv:1008.4225 [hep-ph] [Search INSPIRE].

[13] J. Arrington, K. de Jager, and C. F. Perdrisat, J. Phys.: Conf. Ser. **299**, 012002 (2011) [arXiv:1102.2463 [nucl-ex]] [Search INSPIRE].

[14] P. A. M. Guichon and M. Vanderhaeghen, Phys. Rev. Lett. **91**, 142303 (2003) [arXiv:hep-ph/0306007] [Search INSPIRE].

[15] P. G. Blunden, W. Melnitchouk, and J. A. Tjon, Phys. Rev. Lett. **91**, 142304 (2003) [arXiv:nucl-th/0306076] [Search INSPIRE].

[16] J. Arrington, Phys. Rev. C **71**, 015202 (2005) [arXiv:hep-ph/0408261] [Search INSPIRE].

[17] J. Arrington, W. Melnitchouk, and J. A. Tjon, Phys. Rev. C **76**, 035205 (2007) [arXiv:0707.1861 [nucl-ex]] [Search INSPIRE].

[18] C. E. Carlson and M. Vanderhaeghen, Ann. Rev. Nucl. Part. Sci. **57**, 171 (2007) [arXiv:hep-ph/0701272] [Search INSPIRE].

[19] J. Arrington, P. G. Blunden, and W. Melnitchouk, Prog. Part. Nucl. Phys. **66**, 782 (2011) [arXiv:1105.0951 [nucl-th]] [Search INSPIRE].

[20] S. J. Brodsky and G. R. Farrar, Phys. Rev. D **11**, 1309 (1975).

[21] B. Aubert et al. [BABAR Collaboration], Phys. Rev. D **80**, 052002 (2009) [arXiv:0905.4778 [hep-ex]] [Search INSPIRE].

[22] S. Uehara et al. [Belle Collaboration], Phys. Rev. D **86**, 092007 (2012) [arXiv:1205.3249 [hep-ex]] [Search INSPIRE].

[23] G. D. Cates, C. W. de Jager, S. Riordan, and B. Wojtsekhowski, Phys. Rev. Lett. **106**, 252003 (2011) [arXiv:1103.1808 [nucl-ex]] [Search INSPIRE].

[24] I. A. Qattan and J. Arrington, Phys. Rev. C **86**, 065210 (2012) [arXiv:1209.0683 [nucl-ex]] [Search INSPIRE].

[25] I. A. Qattan, J. Arrington, and A. Alsaad, Phys. Rev. C **91**, 065203 (2015) [arXiv:1502.02872 [nucl-ex]] [Search INSPIRE].

[26] M. Diehl and P. Kroll, Eur. Phys. J. C **73**, 2397 (2013) [arXiv:1302.4604 [hep-ph]] [Search INSPIRE].

[27] I. C. Cloët, G. Eichmann, B. El-Bennich, T. Klahn, and C. D. Roberts, Few Body Syst. **46**, 1 (2009) [arXiv:0812.0416 [nucl-th]] [Search INSPIRE].

[28] C. Crawford et al., Phys. Rev. C **82**, 045211 (2010) [arXiv:1003.0903 [nucl-th]] [Search INSPIRE].

[29] S. Riordan et al., Phys. Rev. Lett. **105**, 262302 (2010) [arXiv:1008.1738 [nucl-ex]] [Search INSPIRE].

[30] G. Eichmann, Phys. Rev. D **84**, 014014 (2011) [arXiv:1104.4505 [hep-ph]] [Search INSPIRE].

[31] M. Rohrmoser, K.-S. Choi, and W. Plessas, arXiv:1110.3665 [hep-ph] [Search INSPIRE].

[32] M. Rohrmoser, K.-S. Choi, and W. Plessas, Few Body Syst. **58**, 83 (2017) [arXiv:1701.07337 [hep-ph]] [Search INSPIRE].

[33] I. C. Cloët and G. A. Miller, Phys. Rev. C **86**, 015208 (2012) [arXiv:1204.4422 [nucl-th]] [Search INSPIRE].

[34] J. O. Gonzalez-Hernandez, S. Liuti, G. R. Goldstein, and K. Kathuria, Phys. Rev. C **88**, 065206 (2013) [arXiv:1206.1876 [hep-ph]] [Search INSPIRE].

[35] D. Chakrabarti and C. Mondal, Eur. Phys. J. C **73**, 2671 (2013) [arXiv:1307.7995 [hep-ph]] [Search INSPIRE].

[36] C. Mondal and D. Chakrabarti, Eur. Phys. J. C **75**, 261 (2015) [arXiv:1501.05489 [hep-ph]] [Search INSPIRE].

[37] C. Mondal, Phys. Rev. D **94**, 073001 (2016) [arXiv:1609.07759 [hep-ph]] [Search INSPIRE].

[38] N. Sharma, Eur. Phys. J. A **52**, 338 (2016) [arXiv:1610.07745 [hep-ph]] [Search INSPIRE].

[39] N. S. Nikkhoo and M. R. Shojaei, Int. J. Mod. Phys. E **24**, 1550086 (2015).

[40] S. J. Brodsky, R. F. Lebed, and V. E. Lyubovitskij, Phys. Lett. B **764**, 174 (2017) [arXiv:1609.06635 [hep-ph]] [Search INSPIRE].

[41] I. T. Obukhovsky, A. Faessler, T. Gutsche, and V. E. Lyubovitskij, J. Phys. G: Nucl. Part. Phys. **41**, 095005 (2014).

[42] D. Chakrabarti and C. Mondal, Eur. Phys. J. C **74**, 2962 (2014) [arXiv:1402.4972 [hep-ph]] [Search INSPIRE].

[43] N. Sharma, Phys. Rev. D **90**, 095024 (2014) [arXiv:1411.7486 [hep-ph]] [Search INSPIRE].

[44] D. I. Diakonov, V. Y. Petrov, and P. V. Pobylitsa, Nucl. Phys. B **306**, 809 (1988).

[45] M. Wakamatsu and H. Yoshiki, Nucl. Phys. A **524**, 561 (1991).

[46] A. Blotz, Diakonov, K. Goeke, N. W. Park, V. Petrov, and P. V. Pobylitsa, Nucl. Phys. A **555**, 765 (1993).

[47] R. Alkofer, H. Reinhardt, and H. Weigel, Phys. Rept. **265**, 139 (1996).

[48] C. V. Christov, A. Blotz, H.-C. Kim, P. Pobylitsa, T. Watabe, Th. Meissner, E. Ruiz Arriola, and K. Goeke, Prog. Part. Nucl. Phys. **37**, 91 (1996) [arXiv:hep-ph/9604441] [Search INSPIRE].

[49] H. Weigel, Lect. Notes Phys. **743**, 1 (2008).

[50] K. Goeke, M. V. Polyakov, and M. Vanderhaeghen, Prog. Part. Nucl. Phys. **47**, 401 (2001) [arXiv:hep-ph/0106012] [Search INSPIRE].

[51] K. Goeke, H.-C. Kim, A. Silva, and D. Urbano, Eur. Phys. J. A **32**, 393 (2007) [arXiv:hep-ph/0608262] [Search INSPIRE].

[52] A. Silva, H.-Ch. Kim, D. Urbano, and K. Goeke, Phys. Rev. D **74**, 054011 (2006) [arXiv:hep-ph/0601239] [Search INSPIRE].

[53] H.-Ch. Kim, A. Blotz, M. V. Polyakov, and K. Goeke, Phys. Rev. D **53**, 4013 (1996) [arXiv:hep-ph/9504363] [Search INSPIRE].

[54] M. Praszałowicz, T. Watabe, and K. Goeke, Nucl. Phys. A **647**, 49 (1999) [arXiv:hep-ph/9806431] [Search INSPIRE].

[55] E. Witten, Nucl. Phys. B **160**, 57 (1979).

[56] E. Witten, Nucl. Phys. B **223**, 422 (1983).

[57] E. Witten, Nucl. Phys. B **223**, 433 (1983).

[58] G. S. Yang, H.-Ch. Kim, M. V. Polyakov, and M. Praszałwicz, Phys. Rev. D **94**, 071502(R) (2016) [arXiv:1607.07089 [hep-ph]] [Search INSPIRE].

[59] H.-Ch. Kim, M. V. Polyakov, and M. Praszałowicz, Phys. Rev. D **96**, 014009 (2017); **96**, 039902 (2017) [addendum] [arXiv:1704.04082 [hep-ph]] [Search INSPIRE].

[60] H.-Ch. Kim, M. V. Polyakov, M. Praszałowicz, and G. S. Yang, Phys. Rev. D **96**, 094021 (2017) [arXiv:1709.04927 [hep-ph]] [Search INSPIRE].

[61] D. Androić et al. [G0 Collaboration], Phys. Rev. Lett. **104**, 012001 (2010) [arXiv:0909.5107 [nucl-ex]] [Search INSPIRE].

[62] X. Ji, J. Phys. G: Nucl. Part. Phys. **24**, 1181 (1998) [arXiv:hep-ph/9807358] [Search INSPIRE].

[63] M. Diehl, Phys. Rept. **388**, 41 (2003) [arXiv:hep-ph/0307382] [Search INSPIRE].

[64] A. V. Belitsky and A. V. Radyushkin, Phys. Rept. **418**, 1 (2005) [arXiv:hep-ph/0504030] [Search INSPIRE].

[65] F. J. Ernst, R. G. Sachs, and K. C. Wali, Phys. Rev. **119**, 1105 (1960).

[66] R. G. Sachs, Phys. Rev. **126**, 2256 (1962).

[67] R. G. Arnold, C. E. Carlson, and F. Gross, Phys. Rev. C **23**, 363 (1981).

[68] G. A. Miller, Phys. Rev. Lett. **99**, 112001 (2007) [arXiv:0705.2409 [nucl-th]] [Search INSPIRE].

[69] G. A. Miller, Ann. Rev. Nucl. Part. Sci. **60**, 1 (2010) [arXiv:1002.0355 [nucl-th]] [Search INSPIRE].

[70] S. Venkat, J. Arrington, G. A. Miller, and X. Zhan, Phys. Rev. C **83**, 015203 (2011) [arXiv:1010.3629 [nucl-th]] [Search INSPIRE].

[71] B. D. Milbrath et al. [Bates FPP Collaboration], Phys. Rev. Lett. **80**, 452 (1998); **82**, 2221 (1999) [erratum] [arXiv:nucl-ex/9712006] [Search INSPIRE].

[72] T. Pospischil et al. [A1 Collaboration], Eur. Phys. J. A **12**, 125 (2001).

[73] G. MacLachlan et al., Nucl. Phys. A **764**, 261 (2006).

[74] M. Paolone et al., Phys. Rev. Lett. **105**, 072001 (2010) [arXiv:1002.2188 [nucl-ex]] [Search INSPIRE].

[75] A. J. R. Puckett et al. [The Jefferson Lab Hall A Collaboration], Phys. Rev. C **85**, 045203 (2012) [arXiv:1102.5737 [nucl-ex]] [Search INSPIRE].

[76] M. K. Jones et al. [Resonance Spin Structure Collaboration], Phys. Rev. C **74**, 035201 (2006) [arXiv:nucl-ex/0606015] [Search INSPIRE].

[77] C. B. Crawford et al., Phys. Rev. Lett. **98**, 052301 (2007) [arXiv:nucl-ex/0609007] [Search INSPIRE].

[78] I. Passchier et al., Phys. Rev. Lett. **82**, 4988 (1999) [arXiv:nucl-ex/9907012] [Search INSPIRE].

[79] H. Zhu et al., Phys. Rev. Lett. **87**, 081801 (2001) [arXiv:nucl-ex/0105001] [Search INSPIRE].

[80] G. Warren et al. [Jefferson Lab E93-026 Collaboration], Phys. Rev. Lett. **92**, 042301 (2004) [arXiv:nucl-ex/0308021] [Search INSPIRE].

[81] E. Geis et al. [BLAST Collaboration], Phys. Rev. Lett. **101**, 042501 (2008) [arXiv:0803.3827 [nucl-ex]] [Search INSPIRE].

[82] C. Herberg et al., Eur. Phys. J. A **5**, 131 (1999).

[83] D. I. Glazier et al., Eur. Phys. J. A **24**, 101 (2005) [arXiv:nucl-ex/0410026] [Search INSPIRE].

[84] B. Plaster et al. [Jefferson Lab E93-038 Collaboration], Phys. Rev. C **73**, 025205 (2006) [arXiv:nucl-ex/0511025] [Search INSPIRE].

[85] J. Bermuth et al., Phys. Lett. B **564**, 199 (2003) [arXiv:nucl-ex/0303015] [Search INSPIRE].

[86] A. Silva, H.-Ch. Kim, and K. Goeke, Phys. Rev. D **65**, 014016 (2001); **66**, 039902 (2002) [erratum] [arXiv:hep-ph/0107185] [Search INSPIRE].

[87] J. J. Kelly, Phys. Rev. C **66**, 065203 (2002) [arXiv:hep-ph/0204239] [Search INSPIRE].

[88] M. Burkardt, Int. J. Mod. Phys. A **18**, 173 (2003) [arXiv:hep-ph/0207047 [hep-ph]] [Search INSPIRE].

[89] C. E. Carlson and M. Vanderhaeghen, Phys. Rev. Lett. **100**, 032004 (2008) [arXiv:0710.0835 [hep-ph]] [Search INSPIRE].